Multi-task learning based P/S wave separation and reverse time migration for VSP

Yanwen Wei, Tsinghua University and National University of Singapore; Yunyue Elita Li, Jizhong Yang and Jingjing Zong, National University of Singapore; Jinwei Fang, China University of Petroleum (Beijing); Haohuan Fu, Tsinghua University*

Summary

P/S wave mode separation is an essential tool for single-mode analysis from multi-component seismic data. Wave separation methods in recorded data require expert knowledge to choose parameters in different shots of data. To make this process automatic, we propose a machine learning-based method to separate P/S waves. This method employs a multi-task neural network that extracts P- and S-potential simultaneously from multi-component VSP data. Targeting at a specific testing dataset, we derive an efficient building strategy to construct training datasets. Synthetic data experiment shows NN trained on our training dataset performs well both in training and testing datasets. We also make further verifications from the view of acoustic reverse time migration. The separated waves by using NN trained on our training datasets have a considerable high-resolution PP and PS imaging.

Introduction

P- and S-wave mode separation is an essential procedure in seismic data analysis. The separation provides an opportunity to analyze single-mode waves from multi-component (Tatham and Goolsbee, 1984). Separated P- and S-waves can be used in acoustic migration, which saves heavy computation and memory space cost in elastic migration (Li et al., 2018).

To separate wave modes correctly in the recorded data, various approaches have been employed, the prior polarization rotation (Greenhalgh et al., 1990; Cho and Spencer, 1992), domain transform (F-K or τ-p) methods (Tatham and Goolsbee, 1984; Dankbaar, 1985, 1987), wave-equation based methods (Dellinger and Etgen, 1990; Sun et al., 2004; Huang and Milkereit, 2007), and statistical methods (Wang et al., 2018; Gao et al., 2013; van Der Baan, 2006; Muijs et al., 2004). However, the whole process of wave separation is time-consuming. An Expert in data processing needs lots of preprocessing to master the main events of the data beforehand (Riedel et al., 2018), and the next step is to separate the data through wave decomposition methods. Furthermore, The difference between near and far offset makes it hard to use the same parameters to separate modes. Most of the time, choosing the parameters is highly dependent on the experience of experts.

To make wave separation for recorded data more automatic, machine learning-based methods, especially Neural Network (NN) based methods, have been applied from different aspects. Kaur et al. (2019) use Generative Adversarial Network to do the elastic wave-mode separation on time slides in a heterogeneous anisotropic medium. Wang and Ma (2019) is searching an NN-based filter to do the P/S-wave decomposition, and to replace the filters used in the wavenumber domain. Wei et al. (2019) focus on separating VSP data directly from the recorded data. Their machine learning-based P-waves separator achieves high training scores on over 40 thousand synthetic data and shows the slight extensibility from data in a flat layer to that in the dipping layer.

In this work, we extend the wave separation method (Wei et al., 2019) to fully utilize multi-component data and extract P- and S-waves simultaneously in a single multi-task network. This abstract shows a successful endeavor to build up training datasets towards a target testing dataset. We exam-

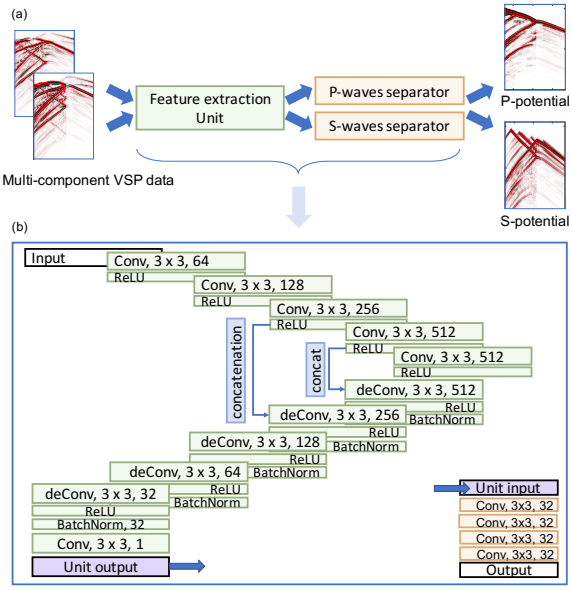

Figure 1: (a) Multi-task schematic diagram and (b) detailed structure of networks for P- and S-waves separation. The network is comprised of a feature extractor and two single-mode separators for P- and S-mode. Feature extractor is shown as the left green structure and two same single-mode separators are shown as the right yellow structure in both (a) and (b). The input of the neural network is multi-component VSP data, and the output is separated P- and S-potential.

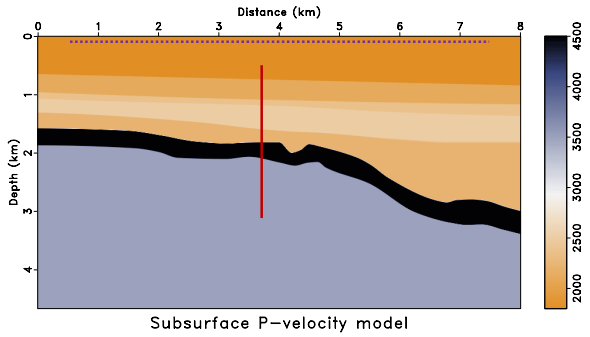

Figure 2: Subsurface P-velocity model and the geometry of acquisition system used in data A. The vertical red solid line denotes the position of well, and horizontal purple dash denotes the position of sources below the surface. The S-velocity model shares the same interface position as that of P-velocity.

ine the effectiveness of our training dataset building strategy by comparing the performance of NN trained on two different datasets. One is produced by our building strategy, and another is the intersection of our training dataset and the target testing dataset. We also analyze the results in raw separated data and their migration imaging by applying acoustic reverse time migration.

Methodology

The workflow of training a machine learning-based wave separator on synthetic seismic data is comprised of

- producing multi-component VSP data, P- and S-waves through elastic forward modeling;
- preprocessing data for training convergence;
- feeding the data into functional neural networks to train and test.

The neural network we used owns a multi-task structure shown in Figure 1, so that it learns to output P- and S-waves simultaneously. The NN consists of two parts, one functions as a critical feature extractor. It receives multi-component of seismic data from the input and extracts features from all of the components. Another part is single-mode separators, separating P- or S-modes from the extracted features.

We apply our data building strategy to this synthetic example. For description convenience, we name the datasets A, B, and C. Dataset-A is used to test the neural networks, of which the separated P- and S-potential is used in migration. The design of dataset-A is an imitation of our target real data. As shown in Figure 2, the well location of dataset-A is at the horizontal position of 3.75 km, and from the depth of 0.5 km to 3 km with 126 receivers. The sources of dataset-A are from horizontal 0.5 km to 7.5 km, in a total number of 140.

Dataset-B is produced under our data building strategy. The aim of dataset-B is trying to build up as much as effective training datasets for networks to learn the P/S wave separation. In this work, under the same subsurface velocity model, we have the interval of sources in dataset-B ten times larger than that in dataset-A, which makes the number of sources for one single well ten times less. Meanwhile, instead of installing well in one place as appeared in dataset-A, we also move the position of well to utilize the same subsurface model fully. Then in dataset-B, we have 15 sources and 16 wells. With one source and one well to produce one set of VSP and separated P- and S-potential records, we have 240 datasets in B in total.

Dataset-C is defined as the intersection of dataset-A and B. The dataset-C shares the same location of well as dataset-A, and the same number of sources as dataset-B.

We use dataset-B and dataset-C for training and dataset-A for testing. The networks used to train on dataset-B and dataset-C have the same structure and hyperparameters. After training, we use dataset-A to test both the NN trained on dataset-B and dataset-C and make the evaluation.

Analysis and evaluation of our data building strategy

We evaluate the testing results of data A from two aspects. First, the relative error between the predicted P- (S-) potential and the referenced P- (S-) potential produced by divergence (curl) calculation. The Average Relative Error (ARE) of training on dataset-C and dataset-A, and testing on dataset-A are shown in Table 1.

Average relative error	*NN trained on Dataset-B*	*NN trained on Dataset-C*
P-potential (train)	0.0201	0.0115
S-potential (train)	0.0528	0.1730
P-potential (test)	0.1632	0.7221
S-potential (test)	0.3013	1.2791

Table 1: The training and testing performance of NN separator trained on dataset-B and C. The testing dataset is A.

From the relative error in Table 1, both dataset-B and C can teach the network to learn their content, while NN trained on dataset-B perform better in testing procedure than NN trained on dataset-C. The different performance in the P- and S-waves also appears in the results between NN trained on dataset-B

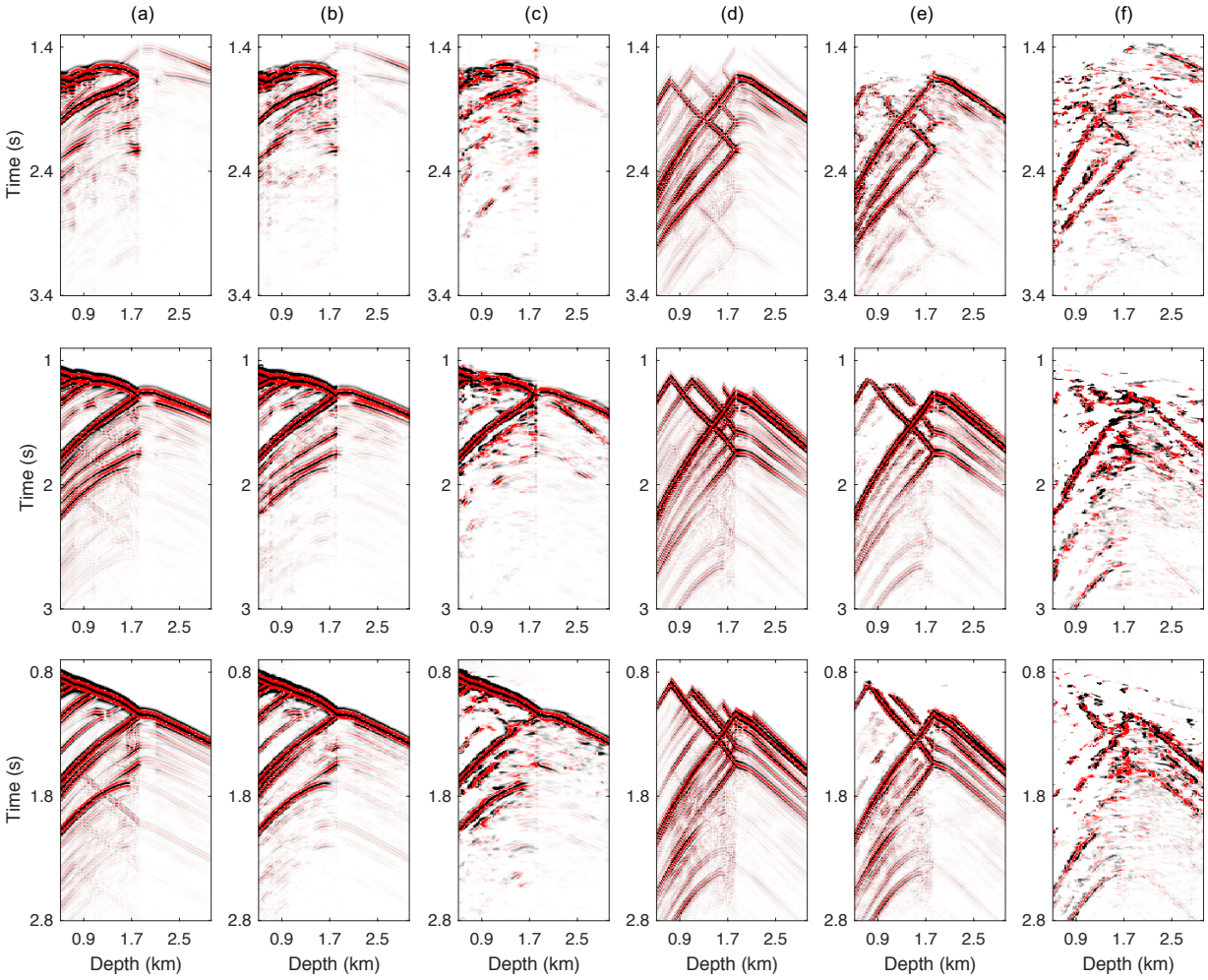

Figure 3: Comparisons of referenced and predicted data. The predicted results of NN are testing results using data A. Rows from top to bottom show shots with different offsets. The top has the largest offset of these three shots, and the bottom has the shortest offset of these three. From view of column, left three columns (a) (b) (c) are P-waves and right three columns (d) (e) (f) are S-waves. Among three columns P- or S-waves, the middle one (b) or (e) is separated waves by NN trained on dataset-B, and left of it (a) or (d) is referenced waves and right of it (c) or (f) is separated waves by NN trained on dataset-C.

and C. The NN trained on dataset-C does a worse separation in S-potential.

More apparent testing results are shown in Figure 3. We pick up typical examples of testing separation among the testing dataset-A. This group of figures compares the separated P-potential (left three columns) and S-potential (right three columns) that produced by three different approaches. Compared the referenced P-potential (a) and S-potential (d) with the separated waves by using NN trained on dataset-B, which are shown in (b) and (e), we can see that NN trained on dataset-B extracts a large percentage of high energy wave event. In this case, P-waves are well separated for first arrivals, transmitted waves, and primary reflections, and show some shortages in separating multiples and other low amplitude events. As a comparison, the separated results produced by NN trained dataset-C, which is (c) and (f) in Figure 3, show fewer well-predicted events. The results of S-waves using trained by dataset-C are worse than P-waves under the same condition. In separated P-waves, most reflections are disappeared except for the reflection on the first layer and the vast contrast layer. Visible fake events also appear in the separated P-potential predicted by NN trained on dataset-C. In the S-waves, only

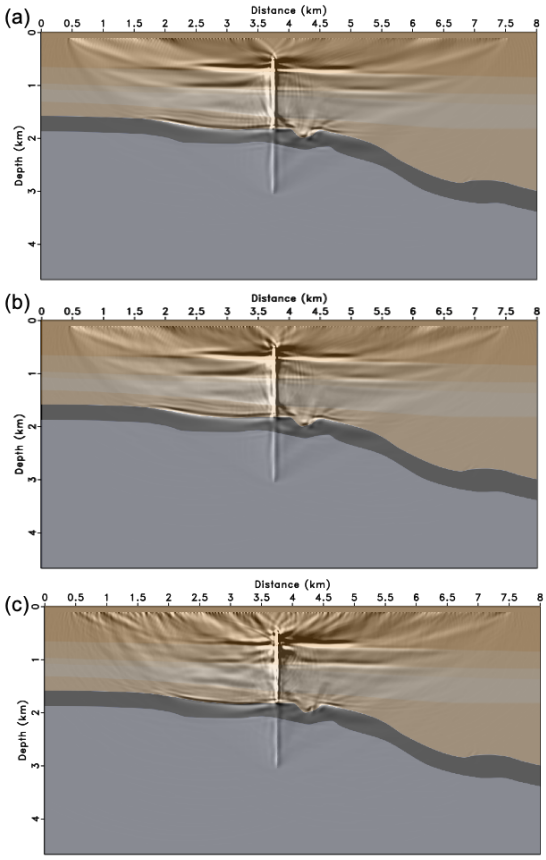

Figure 4: PP-image by reverse time migration using (a) referenced P-potential from divergence calculating of multi-component VSP data; and (b) P-potential predicted by NN trained on dataset-B; (c) P-potential predicted by NN trained on dataset-C.

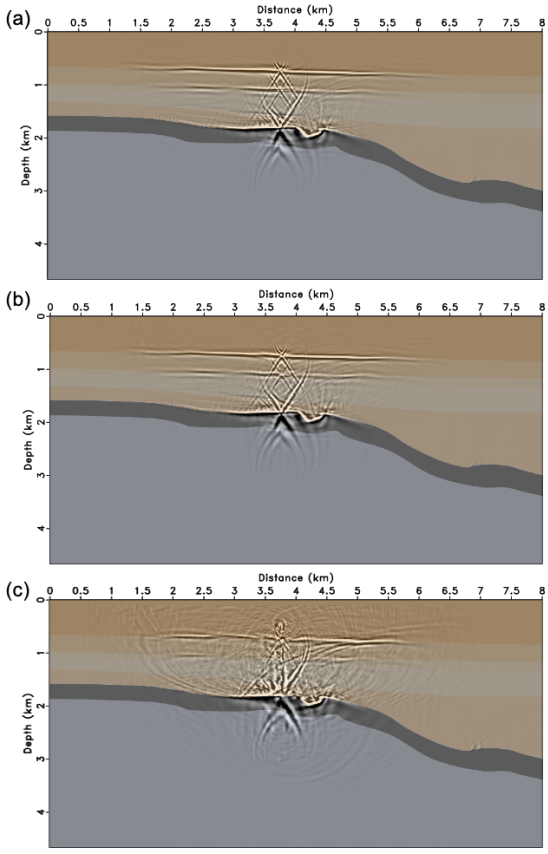

Figure 5: PS-image by reverse time migration using (a) referenced S-potential from curl calculating of multi-component VSP data; and (b) S-potential predicted by NN trained on dataset-B; (c) S-potential predicted by NN trained on dataset-C.

transmitted and reflection events on the large contrast interface can be seen, albeit being discontinuous.

Finally, to fully evaluate how these different separated results influence the subsequent imaging procedure, we use these three kinds of data as the input record data for reverse time migration and obtain the corresponding images. Images are of similar quality between the reference and case B, whereas images produced by case C severely degrade from the reference case, especially for the PS image.

Conclusion

We present a machine learning-based P- and S-wave separation method for VSP. The neural network is a multi-task network. It fully utilizes the multi-component data and derives P- and S-potential simultaneously. To make the NN-based separator performs well, we set up a training data building strategy. This strategy constructs the training dataset on the same subsurface model with a small number of wave simulations by sampling the locations of the receivers. Effectively, this strategy samples many different velocity models without explicitly constructing them. Migration results using the separated P- and S-potential demonstrate that NN-based P/S wave separation has improved accuracy and efficiency for multi-component VSP imaging.

Acknowledgments

The authors acknowledge Petroleum Engineering Professorship for their financial support.

References

Cho, W. H., and T. W. Spencer, 1992, Estimation of polarization and slowness in mixed wavefields: Geophysics, **57**, 805–814.

Dankbaar, J., 1985, Separation of p-and s-waves: Geophysical Prospecting, **33**, 970–986.

———, 1987, Vertical seismic profilingseparation of p-and s-waves: Geophysical Prospecting, **35**, 803–814.

Dellinger, J., and J. Etgen, 1990, Wave-field separation in two-dimensional anisotropic media: Geophysics, **55**, 914–919.

Gao, L., W. Chen, B. Wang, J. Gao, and Q. Bao, 2013, Vsp wavefield separation method based on sparse representation and svt, *in* SEG Technical Program Expanded Abstracts 2013: Society of Exploration Geophysicists, 5102–5106.

Greenhalgh, S., I. Mason, E. Lucas, D. Pant, and R. Eames, 1990, Controlled direction reception filtering of p-and s-waves in τ-p space: Geophysical Journal International, **100**, 221–234.

Huang, J.-w., and B. Milkereit, 2007, Wave-equation-based separation of p-and s-wave modes, *in* SEG Technical Program Expanded Abstracts 2007: Society of Exploration Geophysicists, 2135–2139.

Kaur, H., S. Fomel, and N. Pham, 2019, Elastic wave-mode separation in heterogeneous anisotropic media using deep learning, *in* SEG Technical Program Expanded Abstracts 2019: 2654–2658.

Li, Y. E., Y. Du, J. Yang, A. Cheng, and X. Fang, 2018, Elastic reverse time migration using acoustic propagators: GEOPHYSICS, **83**, S399–S408.

Muijs, R., J. O. Robertsson, and K. Holliger, 2004, Data-driven adaptive decomposition of multicomponent seabed recordings: Geophysics, **69**, 1329–1337.

Riedel, M., C. Cosma, N. Enescu, E. Koivisto, K. Komminaho, K. Vaittinen, and M. Malinowski, 2018, Underground vertical seismic profiling with conventional and fiber-optic systems for exploration in the kylylahti polymetallic mine, eastern finland: Minerals, **8**.

Sun, R., G. A. McMechan, H.-H. Hsiao, and J. Chow, 2004, Separating p-and s-waves in prestack 3d elastic seismograms using divergence and curl: Geophysics, **69**, 286–297.

Tatham, R. H., and D. V. Goolsbee, 1984, Separation of s-wave and p-wave reflections offshore western florida: Geophysics, **49**, 493–508.

van Der Baan, M., 2006, Pp/ps wavefield separation by independent component analysis: Geophysical Journal International, **166**, 339–348.

Wang, W., and J. Ma, 2019, Ps decomposition of isotropic elastic wavefields using cnn-learned filters: 81st EAGE Conference and Exhibition 2019, European Association of Geoscientists & Engineers, 1–5.

Wang, X., J. Chen, L. Gao, and W. Chen, 2018, An iterative zero-offset vsp wavefield separating method based on the error analysis of svd filtering: IEEE Geoscience and Remote Sensing Letters, **15**, 1164–1168.

Wei, Y., H. Fu, Y. E. Li, and J. Yang, 2019, A new p-wave reconstruction method for vsp data using conditional generative adversarial network, *in* SEG Technical Program Expanded Abstracts 2019: 2528–2532.